Nonlocal Shear Deformable Shell Model for Post-Buckling of Axially Compressed Double-Walled Carbon Nanotubes Embedded in an Elastic Matrix

Hui-Shen Shen[1]
Department of Engineering Mechanics,
Shanghai Jiao Tong University,
Shanghai 200030, People's Republic of China;
State Key Laboratory of Ocean Engineering,
Shanghai Jiao Tong University,
Shanghai 200030, People's Republic of China
e-mail: hsshen@mail.sjtu.edu.cn

Chen-Li Zhang
Department of Engineering Mechanics,
Shanghai Jiao Tong University,
Shanghai 200030, People's Republic of China

Buckling and post-buckling analysis is presented for axially compressed double-walled carbon nanotubes (CNTs) embedded in an elastic matrix in thermal environments. The double-walled carbon nanotube is modeled as a nonlocal shear deformable cylindrical shell, which contains small scale effects and van der Waals interaction forces. The surrounding elastic medium is modeled as a tensionless Pasternak foundation. The post-buckling analysis is based on a higher order shear deformation shell theory with the von Kármán–Donnell-type of kinematic nonlinearity. The thermal effects are also included and the material properties are assumed to be temperature-dependent and are obtained from molecular dynamics (MD) simulations. The nonlinear prebuckling deformations of the shell and the initial local point defect, which is simulated as a dimple on the tube wall, are both taken into account. A singular perturbation technique is employed to determine the post-buckling response of the tubes and an iterative scheme is developed to obtain numerical results without using any assumption on the shape of the contact region between the tube and the elastic medium. The small scale parameter e_0a is estimated by matching the buckling loads of CNTs observed from the MD simulation results with the numerical results obtained from the nonlocal shear deformable shell model. Numerical solutions are presented to show the post-buckling behavior of CNTs surrounded by an elastic medium of conventional and tensionless Pasternak foundations. The results show that buckling and post-buckling behavior of CNTs is very sensitive to the small scale parameter e_0a. The results reveal that the unilateral constraint has a significant effect on the post-buckling response of CNTs when the foundation stiffness is sufficiently large.
[DOI: 10.1115/1.4000910]

Keywords: buckling, nanotube, nonlocal shell model, higher order shear deformable shell theory, temperature-dependent properties, initial point defects

1 Introduction

Recently, a new class of promising materials known as carbon nanotubes (CNTs) has drawn considerable attention. Due to their superior material properties, CNTs have many potential applications. Their strong electrical-mechanical coupling make them ideal for sensors [1], while their negative coefficient of thermal expansion more them good candidates for reinforcements in composite materials [2]. Yakobson et al. [3] investigated the buckling of a single walled carbon nanotube (SWCNT) using a traditional continuum shell model and compared it with molecular dynamics simulation. The results show that the continuum shell model could predicate all of the buckling patterns of the SWCNT under axial compression, bending, and torsion that were displayed by their molecular dynamics simulations. Instabilities in CNT-reinforced nanocomposites are of substantial interest and many experiments have observed buckling [4–6]. Ru [7] proposed a continuum shell model to study infinitesimal buckling of double-walled carbon nanotubes (DWCNTs) subjected to axial compression where the effect of surrounding elastic medium and van der Waals forces were taken into account. This model was further extended for double-walled carbon nanotubes and multiwalled carbon nanotubes (MWCNTs) subjected to axial compression [8], torsion [9], bending [10], radial pressure [11], and combined torsion and axial loading [12]. In the aforementioned investigations, however, the shell was assumed to be perfectly bonded to the surrounding medium, and the conventional elastic foundation of the Winkler-type was formulated that means the foundation reacts in compression as well as in tension. Moreover, Kitipornchai et al. [13] extended Ru's model to the linear buckling analysis of a triple-walled carbon nanotube embedded in an elastic matrix, which was modeled as a conventional elastic foundation of Pasternak-type.

CNTs usually do not bond well to elastic matrix such that their interaction is the van der Waals force [14]. However, modeling of CNT and matrix interfaces has been a challenge because it is difficult to account for the van der Waals force in continuum models, and therefore, the van der Waals interaction between CNT and matrix is always neglected in the all above mentioned studies [7–13]. It has been reported that the van der Waals interaction energy can be estimated by using the much applied inverse power model, namely, Lennard–Jones pair potential [15,16], which contains two parts of the short-range repulsive interaction and the long-range attractive interaction [17]. The equilibrium distance between outmost tube and matrix is around 0.34 nm if there are no functional groups between them. It is noted that the buckling deflection of CNTs is infinitesimal even if in the post-buckling re-

[1]Corresponding author.

Contributed by the Applied Mechanics Division of ASME for publication in the JOURNAL OF APPLIED MECHANICS. Manuscript received December 13, 2008; final manuscript received October 8, 2009; published online April 9, 2010. Assoc. Editor: Yonggang Huang.

gion, and the attraction may not exist when the distance between outmost tube and matrix is less than 0.34 nm. In such a case, the local buckling of CNTs is one special class of unilateral buckling problems. This unilateral buckling problem may be modeled as a shell resting on a tensionless elastic foundation. The solution method required to determine the response of such shells on tensionless elastic foundations is quite complicated because the contact region is not known at the outset. The capability to predict the post-buckling response of CNTs with unilateral constraints subjected to axial compression is of prime interest in the nanocomposites analysis. On the other hand, the buckling solutions will lie between the two cases of conventional and tensionless Pasternak foundation models if any the van der Waals attraction exists in the real interface.

There are many continuum shell models for CNTs [7,18,19]. Although the classical continuum models are efficient in CNT buckling analysis through their relatively simple formulae, the small scale effect on the buckling and post-buckling behavior of CNTs cannot be accounted for. Eringen [20] proposed a nonlocal elasticity theory in which the stress state at a given reference point is a function of the strain field at every point in the body, and therefore, the theory of nonlocal continuum mechanics contains information about the long-range forces between atoms, and the internal length scale is introduced into the constitutive equations simply as a material parameter. Modeling a nonlocal thin shell model to study buckling [21–24], vibration [25], and wave propagation [26,27] in CNTs have been identified as an important field of study in recent years.

The nonlinear prebuckling deformation, geometrical nonlinearity and the initial geometric imperfection are the three major effects and must play an important role in the phenomenon of shell buckling. Linear elastic shell theory is simple, but it does not account for the atomistic interactions between carbon atoms in a direct manner. Buckling of CNTs may be beyond linear response [3,28]. CNTs also display strong sensitivity to defects [29]. However, such important effects are not accounted for in any of previous investigations [7–13,21–24]. It is well known the thin shell theory is adequate for cylindrical shells when the radius-to-thickness ratio is greater than 20. As argued previously [18], most CNTs have low values of radius-to-thickness ratio, and therefore, shear deformation shell theory is required. We propose here a nonlocal shear deformable shell model with van der Waals interaction forces, and each tube is described as an individual orthotropic shell and the interlayer friction is negligible between the inner and outer tubes. The surrounding elastic medium is modeled as a tensionless Pasternak foundation that reacts in compression only. The post-buckling analysis is based on a higher order shear deformation shell theory with von Kármán–Donnell-type of kinematic nonlinearity. The thermal effects are also included and the material properties are assumed to be temperature-dependent and are obtained from molecular dynamics (MD) simulations. The nonlinear prebuckling deformations of the shell and the initial local point defect, which is simulated as a dimple on the tube wall, are both taken into account. A singular perturbation technique is employed to determine the post-buckling response of the tubes and an iterative scheme is developed to obtain numerical results without using any assumption on the shape of the contact region between the tube and the elastic medium. The major difference between present model and traditional one is that the present solution includes small scale effects. In the present study, we have three ways to introduce these small scale effects. First, the van der Waals interaction coefficient is calculated by Eq. (11) in the next section to account for the tube size effect. Second, the size-dependent and temperature-dependent material properties are obtained from MD simulations. Third, the small scale parameter e_0a in the governing equations is estimated by matching the buckling loads of CNTs observed from the MD simulation results with the numerical results obtained from the nonlocal shear deformable shell model. The numerical illustrations show the full nonlinear post-buckling response of perfect and imperfect, armchair carbon nanotubes embedded in an elastic medium subjected to axial compression under different sets of environmental conditions.

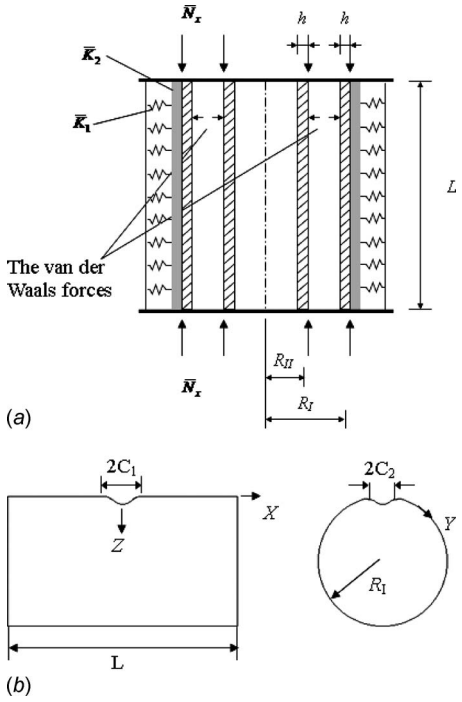

Fig. 1 An elastic shell model for a double-walled carbon nanotube embedded in an elastic matrix: (*a*) geometry and loading case and (*b*) coordinate system and point defect

2 Theoretical Development

Consider a double-walled carbon nanotube modeled as a shell system, which is subjected to axial compressive load in thermal environments. As commonly done [7–13,17,18,21,22,24], the outer and inner tubes are assumed to have the same thickness h and length L, and have mean radii R_I and R_{II}, respectively, as shown in Fig. 1(*a*). Each shell is referred to a coordinate system (X,Y,Z) in which X and Y are in the axial and circumferential directions of the shell and Z is in the direction of the inward normal to the middle surface. The origin of the coordinate system is located at the center of each shell on the middle plane. The corresponding displacements are designated by $\bar{U}$, $\bar{V}$, and $\bar{W}$. $\bar{\Psi}_x$ and $\bar{\Psi}_y$ are the rotations of normals to the middle surface with respect to the Y and X axes, respectively. The shell is assumed to be orthotropic and to be geometrically imperfect. The outer surface of the shell is in contact with an elastic medium that acts as an elastic foundation represented by the Pasternak model, i.e., the reaction of the foundation is assumed to be $p_0=\bar{K}_1\bar{W}-\bar{K}_2\nabla^2\bar{W}$, where p_0 is the force per unit area, $\bar{K}_1$ is the Winkler foundation stiffness and $\bar{K}_2$ is the shearing layer stiffness of the foundation, and ∇^2 is the Laplace operator in X and Y. This reaction, however, is only compressive and occurs only when p_0 is positive. Denoting the initial local defect by $\bar{W}^*(X,Y)$, let $\bar{W}(X,Y)$ be the transverse deflection of each tube, and $\bar{F}(X,Y)$ be the stress function for the stress resultants defined by $\bar{N}_x=\bar{F}_{,YY}$, $\bar{N}_y=\bar{F}_{,XX}$, and $\bar{N}_{xy}=\bar{F}_{,XY}$, where a comma denotes partial differentiation with respect to the corresponding coordinates.

According to nonlocal elasticity, the constitutive relations of nonlocal elasticity for 3D problems are expressed as

$$(1-\tau^2L^2\nabla^2)\sigma_{ij}=C_{ijkl}\varepsilon_{kl} \tag{1}$$

where $\tau=e_0a/L$. σ_{ij} and ε_{ij} are the stress and strain tensors, and C_{ijkl} is the elastic module tensor of classical isotropic elasticity, e_0 is a material constant, and a and L are the internal and external characteristic lengths, respectively.

Reddy and Liu [30] developed a simple higher order shear deformation shell theory. Their theory assumes that the transverse shear strains are parabolically distributed across the shell thickness. The advantages of this theory over the first order shear deformation shell theory are that the number of independent unknowns is the same as in the first order shear deformation theory, and no shear correction factors are required. Applying Eq. (1) to Reddy's higher order shear deformation shell theory, the Kármán–Donnell-type nonlinear differential equations for the outer tube, including small scale effects, van der Waals interaction forces, and thermal effects, have readily been derived and can be expressed in terms of a stress function $\bar{F}_I$, two rotations $\bar{\Psi}_{xI}$ and $\bar{\Psi}_{yI}$, and two transverse displacements $\bar{W}_I$ and $\bar{W}_{II}$, along with the initial geometric imperfection $\bar{W}_I^*$. They are

$$\tilde{L}_{11}(\bar{W}_I)-\tilde{L}_{12}(\bar{\Psi}_{xI})-\tilde{L}_{13}(\bar{\Psi}_{yI})-\tilde{L}_{16}(\bar{M}^T)-\frac{1}{R_I}\bar{F}_{I,xx}=(1-\tau^2L^2\nabla^2)\times[\tilde{L}(\bar{W}_I+\bar{W}_I^*,\bar{F}_I)-H(\bar{W})[\bar{K}_1\bar{W}_I-\bar{K}_2\nabla^2\bar{W}_I]+C(\bar{W}_{II}-\bar{W}_I)] \tag{2}$$

$$\tilde{L}_{21}(\bar{F}_I)-\tilde{L}_{25}(\bar{N}^T)+\frac{1}{R_I}\bar{W}_{I,xx}=-\frac{1}{2}\tilde{L}(\bar{W}_I+2\bar{W}_I^*,\bar{W}_I) \tag{3}$$

$$\tilde{L}_{31}(\bar{W}_I)+\tilde{L}_{32}(\bar{\Psi}_{xI})-\tilde{L}_{33}(\bar{\Psi}_{yI})-\tilde{L}_{36}(\bar{S}^T)=0 \tag{4}$$

$$\tilde{L}_{41}(\bar{W}_I)-\tilde{L}_{42}(\bar{\Psi}_{xI})+\tilde{L}_{43}(\bar{\Psi}_{yI})-\tilde{L}_{46}(\bar{S}^T)=0 \tag{5}$$

and for the inner tube they are

$$\tilde{L}_{11}(\bar{W}_{II})-\tilde{L}_{12}(\bar{\Psi}_{xII})-\tilde{L}_{13}(\bar{\Psi}_{yII})-\tilde{L}_{16}(\bar{M}^T)-\frac{1}{R_{II}}\bar{F}_{II,xx}=(1-\tau^2L^2\nabla^2)\left[\tilde{L}(\bar{W}_{II}+\bar{W}_{II}^*,\bar{F}_{II})-\frac{R_I}{R_{II}}C(\bar{W}_{II}-\bar{W}_I)\right] \tag{6}$$

$$\tilde{L}_{21}(\bar{F}_{II})-\tilde{L}_{25}(\bar{N}^T)+\frac{1}{R_{II}}\bar{W}_{II,xx}=-\frac{1}{2}\tilde{L}(\bar{W}_{II}+2\bar{W}_{II}^*,\bar{W}_{II}) \tag{7}$$

$$\tilde{L}_{31}(\bar{W}_{II})+\tilde{L}_{32}(\bar{\Psi}_{xII})-\tilde{L}_{33}(\bar{\Psi}_{yII})-\tilde{L}_{36}(\bar{S}^T)=0 \tag{8}$$

$$\tilde{L}_{41}(\bar{W}_{II})-\tilde{L}_{42}(\bar{\Psi}_{xII})+\tilde{L}_{43}(\bar{\Psi}_{yII})-\tilde{L}_{46}(\bar{S}^T)=0 \tag{9}$$

where

$$\tilde{L}_{16}(\bar{M}^T)=\frac{\partial^2}{\partial X^2}(\bar{M}_x^T)+2\frac{\partial^2}{\partial X\,\partial Y}(\bar{M}_{xy}^T)+\frac{\partial^2}{\partial Y^2}(\bar{M}_y^T)$$

$$\tilde{L}_{25}(\bar{N}^T)=\left(A_{12}^*\frac{\partial^2}{\partial X^2}+A_{11}^*\frac{\partial^2}{\partial Y^2}\right)(\bar{N}_x^T)-A_{66}^*\frac{\partial^2}{\partial X\,\partial Y}(\bar{N}_{xy}^T)+\left(A_{22}^*\frac{\partial^2}{\partial X^2}+A_{12}^*\frac{\partial^2}{\partial Y^2}\right)(\bar{N}_y^T)$$

$$\tilde{L}_{36}(\bar{S}^T)=\frac{\partial}{\partial X}(\bar{S}_x^T)+\frac{\partial}{\partial Y}(\bar{S}_{xy}^T)$$

$$\tilde{L}_{46}(\bar{S}^T)=\frac{\partial}{\partial X}(\bar{S}_{xy}^T)+\frac{\partial}{\partial Y}(\bar{S}_y^T) \tag{10}$$

Note that the geometric nonlinearity in the von Kármán sense is given in terms of $\tilde{L}(\,)$ in Eqs. (2), (3), (6), and (7), and the other linear operators $\tilde{L}_{ij}(\,)$ are defined as in Ref. [31]. Small scale parameter e_0a is included in Eqs. (2) and (6). The nonlocal shear deformable shell model described by Eqs. (2)–(9) reduces to the local shear deformable shell model when the small scale parameter e_0a vanishes. Since each tube is assumed to be orthotropic, the stretching-bending coupling is zero-valued, i.e., $B_{ij}=E_{ij}=0$ $(i,j=1,2,6)$ in the present case. Equations (2)–(9) are coupled and should be solved simultaneously.

It is assumed that the van der Waals interaction forces between the inner and outer shells are linearly proportional to the buckling deflection. This assumption is reasonably well when the interlayer distance is less than 0.425 nm. As will be seen later in Sec. 4, this condition can be satisfied in the numerical analysis. In Eqs. (2) and (6), C is the van der Waals interaction coefficient, which was assumed to be a constant and approximately taken to be 61.9917 GPa/nm in Ref. [7] and 99.1867 GPa/nm in Ref. [32]. In fact, van der Waals forces are a kind of weak interactions between atoms that are not directly bonded together in the same molecular. In the present work, C is estimated as the second derivative of the van der Waals energy-interlayer spacing. To account for the tube size effect and to include two parts of the repulsive and attractive interactions, we have [33]

$$C=\frac{1001\pi\varepsilon_0\sigma_0^{12}R_{II}}{6d^4R_I^{13}}\int_0^{\pi}\frac{1}{[1-2\gamma_0\cos\theta+\gamma_0^2]^{13/2}}d\theta-\frac{560\pi\varepsilon_0\sigma_0^6R_{II}}{9d^4R_I^7}\int_0^{\pi}\frac{1}{[1-2\gamma_0\cos\theta+\gamma_0^2]^{7/2}}d\theta \tag{11}$$

where $\gamma_0=R_{II}/R_I$, $d=0.142$ nm is the C-C bond length, ε_0 is the depth of the potential, and σ_0 is a parameter that is determined by the equilibrium distance.

Because the outer tube is not attached to the foundation, tensile stresses may not occur between the tube and the foundation at any point when the distance between outer tube and foundation is less than 0.34 nm and therefore the tube may lift off the foundation over certain intervals. As mentioned before, the tensile stress will exist when the separation is slightly larger than the equilibrium distance if the van der Waals interaction between the matrix and CNT is considered. As will be seen later in Sec. 4, the buckling deflection of outer tube is much less than 0.34 nm, and in such a case, the tensile stresses due to van der Waals interaction do not exist between the matrix and CNT. A compressive reaction occurs when there is a contact between the tube and the foundation. The reaction will be reduced to zero when a separation at the contact develops. This characteristics of the foundation is taken into account in Eq. (2) by introducing a contact function defined by

$$H(\bar{W})=\begin{cases}1 & \text{for } p_0=\bar{K}_1\bar{W}-\bar{K}_2\nabla^2\bar{W}>0\\ 0 & \text{for } p_0=\bar{K}_1\bar{W}-\bar{K}_2\nabla^2\bar{W}\le 0\end{cases} \tag{12}$$

and for a conventional Pasternak foundation we always have $H(\bar{W})=1$.

It is assumed that the effective Young's moduli E_{11} and E_{22}, shear moduli G_{12}, G_{13}, and G_{23}, and thermal expansion coefficients α_{11} and α_{22} of each tube are temperature-dependent, whereas Poisson's ratio ν_{12} depends weakly on temperature change and is assumed to be a constant. The thermal forces $\bar{N}^T$, moments $\bar{M}^T$ and $\bar{S}^T$, and higher order moments $\bar{P}^T$ caused by elevated temperature are defined by

$$\begin{bmatrix}\bar{N}_x^T & \bar{M}_x^T & \bar{P}_x^T\\ \bar{N}_y^T & \bar{M}_y^T & \bar{P}_y^T\\ \bar{N}_{xy}^T & \bar{M}_{xy}^T & \bar{P}_{xy}^T\end{bmatrix}=\int_{-h/2}^{+h/2}\begin{bmatrix}A_x(T)\\ A_y(T)\\ A_{xy}(T)\end{bmatrix}(1,Z,Z^3)\Delta T dZ \tag{13a}$$

and

$$\begin{bmatrix} \bar{S}_x^T \\ \bar{S}_y^T \\ \bar{S}_{xy}^T \end{bmatrix} = \begin{bmatrix} \bar{M}_x^T \\ \bar{M}_y^T \\ \bar{M}_{xy}^T \end{bmatrix} - \frac{4}{3h^2} \begin{bmatrix} \bar{P}_x^T \\ \bar{P}_y^T \\ \bar{P}_{xy}^T \end{bmatrix} \tag{13b}$$

where $\Delta T = T - T_0$ is temperature rise from some reference temperature T_0 at which there are no thermal strains, and

$$\begin{bmatrix} A_x(T) \\ A_y(T) \\ A_{xy}(T) \end{bmatrix} = - \begin{bmatrix} \bar{Q}_{11}(T) & \bar{Q}_{12}(T) & \bar{Q}_{16}(T) \\ \bar{Q}_{12}(T) & \bar{Q}_{22}(T) & \bar{Q}_{26}(T) \\ \bar{Q}_{16}(T) & \bar{Q}_{26}(T) & \bar{Q}_{66}(T) \end{bmatrix} \begin{bmatrix} 1 & 0 \\ 0 & 1 \\ 0 & 0 \end{bmatrix} \begin{bmatrix} \alpha_{11}(T) \\ \alpha_{22}(T) \end{bmatrix} \tag{14}$$

in which $\bar{Q}_{ij}(T) = Q_{ij}(T)$ and

$$Q_{11}(T) = \frac{E_{11}(T)}{1 - \nu_{12}\nu_{21}}, \quad Q_{22}(T) = \frac{E_{22}(T)}{1 - \nu_{12}\nu_{21}}, \quad Q_{12}(T) = \frac{\nu_{21}E_{11}(T)}{1 - \nu_{12}\nu_{21}}$$

$$Q_{16} = Q_{26} = 0, \quad Q_{44}(T) = G_{23}(T), \quad Q_{55}(T) = G_{13}(T),$$

$$Q_{66}(T) = G_{12}(T) \tag{15}$$

From Eqs. (13) and (14) the thermal force $\bar{N}_{xy}^T$, the thermal moments $\bar{M}^T$, and the higher order moments $\bar{P}^T$ are all zero-valued, and $\bar{N}_x^T$ and $\bar{N}_y^T$ are both constants, so that $\tilde{L}_{25}(\bar{N}^T) = \tilde{L}_{16}(\bar{M}^T) = \tilde{L}_{36}(\bar{S}^T) = \tilde{L}_{46}(\bar{S}^T) = 0$.

The point defect, like vacancy, is a basic and important geometric imperfection in CNTs [34], which may be modeled as a dimple in the outer tube or in both outer and inner tubes. We assume that the point defect located in the center of the CNTs can be expressed as

$$\bar{W}^*(X,Y) = A_m \exp\left(- \left| \frac{X}{C_1} \right| - \left| \frac{Y}{C_2} \right| \right) \tag{16}$$

where A_m is a small parameter characterizing the amplitude of the initial defect and C_1 and C_2 characterize the half-width of the region of the dimple, as shown in Fig. 1(*b*).

The two end edges of both outer and inner tubes are assumed to be simply supported or clamped, so that the boundary conditions are $X = \pm L/2$

$$\bar{W} = \bar{V} = \bar{\Psi}_y = 0 \tag{17a}$$

$$\bar{M}_x = \bar{P}_x = 0 \quad \text{(simply supported)} \tag{17b}$$

$$\bar{\Psi}_x = 0 \quad \text{(clamped)} \tag{17c}$$

$$\int_0^{2\pi R_I} \bar{N}_{xI} dY + \int_0^{2\pi R_{II}} \bar{N}_{xII} dY + 2\pi(R_I + R_{II}) h \sigma_x = 0 \tag{17d}$$

where σ_x is the average axial compressive stress, and $\bar{M}_x$ is the bending moment and $\bar{P}_x$ is higher order moment, as defined in Ref. [30]. Also we have the closed (or periodicity) condition for each tube

$$\int_0^{2\pi R_J} \frac{\partial \bar{V}}{\partial Y} dY = 0 \quad (J = I, II) \tag{18a}$$

or

$$\int_0^{2\pi R_J} \left[A_{22}^* \frac{\partial^2 \bar{F}}{\partial X^2} + A_{12}^* \frac{\partial^2 \bar{F}}{\partial Y^2} + \frac{\bar{W}}{R_J} - \frac{1}{2}\left(\frac{\partial \bar{W}}{\partial Y} \right)^2 - \frac{\partial \bar{W}}{\partial Y} \frac{\partial \bar{W}_J^*}{\partial Y} - (A_{12}^* \bar{N}_x^T + A_{22}^* \bar{N}_y^T) \right] dY = 0 \tag{18b}$$

Because of Eq. (18*a*), the in-plane boundary condition $\bar{V} = 0$ (at $X = \pm L/2$) is not needed in Eq. (17*a*).

It is assumed that the end-shortening displacements of the outer and inner tubes are identical. The average end-shortening relationship of each shell is defined as

$$\frac{\Delta_x}{L} = - \frac{1}{2\pi R_J L} \int_0^{2\pi R_J} \int_{-L/2}^{+L/2} \frac{\partial \bar{U}}{\partial X} dX dY$$

$$= - \frac{1}{2\pi R_J L} \int_0^{2\pi R_J} \int_{-L/2}^{+L/2} \left[A_{11}^* \frac{\partial^2 \bar{F}}{\partial Y^2} + A_{12}^* \frac{\partial^2 \bar{F}}{\partial X^2} - \frac{1}{2}\left(\frac{\partial \bar{W}}{\partial X} \right)^2 - \frac{\partial \bar{W}}{\partial X} \frac{\partial \bar{W}_J^*}{\partial X} - (A_{11}^* \bar{N}_x^T + A_{12}^* \bar{N}_y^T) \right] dX dY (J = I, II) \tag{19}$$

where Δ_x is the shell end-shortening displacement in the X direction.

In the above equations and in what follows, the reduced stiffness matrices $[A_{ij}^*]$, $[D_{ij}^*]$, $[F_{ij}^*]$ $(i,j = 1,2,4,5,6)$, and $[H_{ij}^*]$ $(i,j = 1,2,6)$ are functions of temperature, determined through relationship [18]

$$\mathbf{A}^* = \mathbf{A}^{-1}, \quad \mathbf{D}^* = \mathbf{D}, \quad \mathbf{F}^* = \mathbf{F}, \quad \mathbf{H}^* = \mathbf{H} \tag{20a}$$

where A_{ij}, D_{ij}, etc., are the shell stiffnesses, defined by

$$(A_{ij}, D_{ij}, F_{ij}, H_{ij}) = \int_{-h/2}^{+h/2} Q_{ij}(T)(1, Z^2, Z^4, Z^6) dZ \tag{20b}$$

3 Solution Methodology

Having developed the theory, we are in a position to solve Eqs. (2)–(9) with boundary conditions (17). Before carrying out the solution process, it is convenient first to define the following dimensionless quantities (with γ_{ijk} in the Appendix are defined, as in Ref. [31]), in which the alternative forms k_1 and k_2 are not needed until the numerical examples are considered

$$x = \pi \frac{X}{L}, \quad y = \frac{Y}{R_I}, \quad \beta = \frac{L}{\pi R_I}, \quad \varepsilon = \frac{\pi^2 R_I}{L^2} [D_{11}^* D_{22}^* A_{11}^* A_{22}^*]^{1/4},$$

$$\gamma_0 = \frac{R_{II}}{R_I}, \quad C_0 = \frac{CL^4}{\pi^4 D_{11}^*}$$

$$\gamma_{14} = \left[\frac{D_{22}^*}{D_{11}^*} \right]^{1/2}, \quad \gamma_{24} = \left[\frac{A_{11}^*}{A_{22}^*} \right]^{1/2}, \quad \gamma_5 = - \frac{A_{12}^*}{A_{22}^*},$$

$$(\gamma_{T1}, \gamma_{T2}) = (A_x^T, A_y^T) R_I \left[\frac{A_{11}^* A_{22}^*}{D_{11}^* D_{22}^*} \right]^{1/4}$$

$$(K_1, k_1) = \bar{K}_1 \left(\frac{L^4}{\pi^4 D_{11}^*}, \frac{R_I^4}{E_0 h^3} \right),$$

$$(K_2, k_2) = \bar{K}_2 \left(\frac{L^2}{\pi^2 D_{11}^*}, \frac{R_I^2}{E_0 h^3} \right), \quad (\gamma_{C1}, \gamma_{C2}) = \left(\frac{L}{\pi C_1}, \frac{R_I}{C_2} \right)$$

$$(W, W^*) = \varepsilon \frac{(\bar{W}, \bar{W}^*)}{[D_{11}^* D_{22}^* A_{11}^* A_{22}^*]^{1/4}}, \quad F = \varepsilon^2 \frac{\bar{F}}{[D_{11}^* D_{22}^*]^{1/2}},$$

$$(\Psi_x, \Psi_y) = \varepsilon^2 \frac{L}{\pi} \frac{(\bar{\Psi}_x, \bar{\Psi}_y)}{[D_{11}^* D_{22}^* A_{11}^* A_{22}^*]^{1/4}}$$

$$(M_x, P_x) = \varepsilon^2 \frac{L^2}{\pi^2} \frac{1}{D_{11}^* [D_{11}^* D_{22}^* A_{11}^* A_{22}^*]^{1/4}} \left(\bar{M}_x, \frac{4}{3h^2} \bar{P}_x \right)$$

$$\lambda_p = \frac{\sigma_x R_I h}{2}\left[\frac{A_{11}^* A_{22}^*}{D_{11}^* D_{22}^*}\right]^{1/4}, \quad \delta_p = \left(\frac{\Delta_x}{L}\right)\frac{R_I}{2[D_{11}^* D_{22}^* A_{11}^* A_{22}^*]^{1/4}} \tag{21}$$

in which E_0 is the reference value of E_{22} at $T=300$ K, and $A_x^T = A_y^T$ are defined by

$$\begin{bmatrix} A_x^T \\ A_y^T \end{bmatrix} = -\int_{-h/2}^{h/2} \begin{bmatrix} A_x \\ A_y \end{bmatrix} dZ \tag{22}$$

The nonlinear Eqs. (2)–(9) may then be written in dimensionless form as

$$\begin{aligned}\varepsilon^2[L_{11}(W_I) + (1-\tau^2\pi^2\nabla^2)H(W)(K_1 W_I - K_2\nabla^2 W_I) - (1 - \tau^2\pi^2\nabla^2)C_0(W_{II} - W_I)] - \varepsilon L_{12}(\Psi_{xI}) - \varepsilon L_{13}(\Psi_{yI}) - \gamma_{14}F_{I,xx} \\ = (1-\tau^2\pi^2\nabla^2)[\gamma_{14}\beta^2 L(W_I + W_I^*, F_I)]\end{aligned} \tag{23}$$

$$L_{21}(F_I) + \gamma_{24}W_{I,xx} = -\tfrac{1}{2}\gamma_{24}\beta^2 L(W_I + 2W_I^*, W_I) \tag{24}$$

$$\varepsilon L_{31}(W_I) + L_{32}(\Psi_{xI}) - L_{33}(\Psi_{yI}) = 0 \tag{25}$$

$$\varepsilon L_{41}(W_I) - L_{42}(\Psi_{xI}) + L_{43}(\Psi_{yI}) = 0 \tag{26}$$

and

$$\begin{aligned}\varepsilon^2[\gamma_0 L_{11}(W_{II}) + (1-\tau^2\pi^2\nabla^2)C_0(W_{II} - W_I)] - \varepsilon\gamma_0 L_{12}(\Psi_{xII}) - \varepsilon\gamma_0 L_{13}(\Psi_{yII}) - \gamma_{14}F_{II,xx} \\ = (1-\tau^2\pi^2\nabla^2)[\gamma_0\gamma_{14}\beta^2 L(W_{II} + W_{II}^*, F_{II})]\end{aligned} \tag{27}$$

$$\gamma_0 L_{21}(F_{II}) + \gamma_{24}W_{II,xx} = -\tfrac{1}{2}\gamma_0\gamma_{24}\beta^2 L(W_{II} + 2W_{II}^*, W_{II}) \tag{28}$$

$$\varepsilon L_{31}(W_{II}) + L_{32}(\Psi_{xII}) - L_{33}(\Psi_{yII}) = 0 \tag{29}$$

$$\varepsilon L_{41}(W_{II}) - L_{42}(\Psi_{xII}) + L_{43}(\Psi_{yII}) = 0 \tag{30}$$

where all dimensionless linear operators $L_{ij}(\,)$ and nonlinear operators $L(\,)$ are defined, as in Ref. [31].

The boundary conditions of Eq. (17) become $x = \pm\pi/2$

$$W = \Psi_y = 0 \tag{31a}$$

$$M_x = P_x = 0 \quad \text{(simply supported)} \tag{31b}$$

$$\Psi_x = 0 \quad \text{(clamped)} \tag{31c}$$

$$\frac{1}{2\pi}\int_0^{2\pi}\beta^2\frac{\partial^2 F_I}{\partial y^2}dy + \frac{1}{2\pi}\int_0^{2\pi\gamma_0}\beta^2\frac{\partial^2 F_{II}}{\partial y^2}dy + 2\lambda_p\varepsilon(1+\gamma_0) = 0 \tag{31d}$$

and the closed condition of Eq. (18*b*) becomes

$$\int_0^{2\pi}\left[\left(\frac{\partial^2 F_I}{\partial x^2} - \gamma_5\beta^2\frac{\partial^2 F_I}{\partial y^2}\right) + \gamma_{24}W_I - \frac{1}{2}\gamma_{24}\beta^2\left(\frac{\partial W_I}{\partial y}\right)^2 - \gamma_{24}\beta^2\frac{\partial W_I}{\partial y}\frac{\partial W_I^*}{\partial y} + \varepsilon(\gamma_{T2} - \gamma_5\gamma_{T1})\Delta T\right]dy = 0 \tag{32}$$

The unit end-shortening relationship becomes

$$\delta_p = -\frac{1}{4\pi^2\gamma_{24}}\varepsilon^{-1}\int_0^{2\pi}\int_{-\pi/2}^{+\pi/2}\left[\left(\gamma_{24}^2\beta^2\frac{\partial^2 F_I}{\partial y^2} - \gamma_5\frac{\partial^2 F_I}{\partial x^2}\right) - \frac{1}{2}\gamma_{24}\left(\frac{\partial W_I}{\partial x}\right)^2 - \gamma_{24}\frac{\partial W_I}{\partial x}\frac{\partial W_I^*}{\partial x} + \varepsilon(\gamma_{24}^2\gamma_{T1} - \gamma_5\gamma_{T2})\Delta T\right]dxdy \tag{33a}$$

$$= -\frac{1}{4\pi^2\gamma_0\gamma_{24}}\varepsilon^{-1}\int_0^{2\pi\gamma_0}\int_{-\pi/2}^{+\pi/2}\left[\left(\gamma_{24}^2\beta^2\frac{\partial^2 F_{II}}{\partial y^2} - \gamma_5\frac{\partial^2 F_{II}}{\partial x^2}\right) - \frac{1}{2}\gamma_{24}\left(\frac{\partial W_{II}}{\partial x}\right)^2 - \gamma_{24}\frac{\partial W_{II}}{\partial x}\frac{\partial W_{II}^*}{\partial x} + \varepsilon(\gamma_{24}^2\gamma_{T1} - \gamma_5\gamma_{T2})\Delta T\right]dxdy \tag{33b}$$

In Eq. (21), we introduce an important parameter ε. As has been shown in Refs. [18,33], CNTs will have large values of $\bar{Z}(=L^2/R_I h)$, so that we always have $\varepsilon \ll 1$. When $\varepsilon < 1$, both Eqs. (23)–(30) are of the boundary layer type and may then be solved by means of a singular perturbation technique. The essence of this procedure, in the present case, is to assume that

$$\begin{aligned} W &= w(x,y,\varepsilon) + \tilde{W}(x,\xi,y,\varepsilon) + \hat{W}(x,\zeta,y,\varepsilon) \\ F &= f(x,y,\varepsilon) + \tilde{F}(x,\xi,y,\varepsilon) + \hat{F}(x,\zeta,y,\varepsilon) \\ \Psi_x &= \psi_x(x,y,\varepsilon) + \tilde{\Psi}_x(x,\xi,y,\varepsilon) + \hat{\Psi}_x(x,\zeta,y,\varepsilon) \\ \Psi_y &= \psi_y(x,y,\varepsilon) + \tilde{\Psi}_y(x,\xi,y,\varepsilon) + \hat{\Psi}_y(x,\zeta,y,\varepsilon) \end{aligned} \tag{34}$$

where ε is a small perturbation parameter (provided $\bar{Z} > 2.96$), as defined in Eq. (21) and $w(x,y,\varepsilon)$, $f(x,y,\varepsilon)$, $\psi_x(x,y,\varepsilon)$, and $\psi_y(x,y,\varepsilon)$, are called regular solutions of the shell; $\tilde{W}(x,\xi,y,\varepsilon)$, $\tilde{F}(x,\xi,y,\varepsilon)$, $\tilde{\Psi}_x(x,\xi,y,\varepsilon)$, $\tilde{\Psi}_y(x,\xi,y,\varepsilon)$ and $\hat{W}(x,\zeta,y,\varepsilon)$, $\hat{F}(x,\zeta,y,\varepsilon)$, $\hat{\Psi}_x(x,\zeta,y,\varepsilon)$, $\hat{\Psi}_y(x,\zeta,y,\varepsilon)$ are the boundary layer solutions near the $x = \pm\pi/2$ edges, respectively; and ξ and ζ are the boundary layer variables, defined as

$$\xi = (\pi/2 + x)/\sqrt{\varepsilon}, \quad \zeta = (\pi/2 - x)/\sqrt{\varepsilon} \tag{35}$$

This means for isotropic cylindrical shells the width of the boundary layers is of order $\sqrt{Rh}$. In Eq. (34) the regular and boundary layer solutions are taken in the forms of perturbation expansions as

$$\begin{aligned} w(x,y,\varepsilon) &= \sum_{j=1}\varepsilon^{j/2}w_{j/2}(x,y), \\ f(x,y,\varepsilon) &= \sum_{j=0}\varepsilon^{j/2}f_{j/2}(x,y), \\ \psi_x(x,y,\varepsilon) &= \sum_{j=1}\varepsilon^{j/2}(\psi_x)_{j/2}(x,y), \\ \psi_y(x,y,\varepsilon) &= \sum_{j=1}\varepsilon^{j/2}(\psi_y)_{j/2}(x,y) \end{aligned} \tag{36a}$$

$$\begin{aligned} \tilde{W}(x,\xi,y,\varepsilon) &= \sum_{j=0}\varepsilon^{j/2+1}\tilde{W}_{j/2+1}(x,\xi,y), \\ \tilde{F}(x,\xi,y,\varepsilon) &= \sum_{j=0}\varepsilon^{j/2+2}\tilde{F}_{j/2+2}(x,\xi,y), \\ \tilde{\Psi}_x(x,\xi,y,\varepsilon) &= \sum_{j=0}\varepsilon^{(j+3)/2}(\tilde{\Psi}_x)_{(j+3)/2}(x,\xi,y), \\ \tilde{\Psi}_y(x,\xi,y,\varepsilon) &= \sum_{j=0}\varepsilon^{j/2+2}(\tilde{\Psi}_y)_{j/2+2}(x,\xi,y) \end{aligned} \tag{36b}$$

$$\begin{aligned} \hat{W}(x,\zeta,y,\varepsilon) &= \sum_{j=0}\varepsilon^{j/2+1}\hat{W}_{j/2+1}(x,\zeta,y), \\ \hat{F}(x,\zeta,y,\varepsilon) &= \sum_{j=0}\varepsilon^{j/2+2}\hat{F}_{j/2+2}(x,\zeta,y), \end{aligned}$$

$$\hat{\Psi}_x(x,\zeta,y,\varepsilon) = \sum_{j=0} \varepsilon^{(j+3)/2}(\hat{\Psi}_x)_{(j+3)/2}(x,\zeta,y),$$

$$\hat{\Psi}_y(x,\zeta,y,\varepsilon) = \sum_{j=0} \varepsilon^{j/2+2}(\hat{\Psi}_y)_{j/2+2}(x,\zeta,y) \tag{36c}$$

For classical linear buckling of cylindrical shell subjected to axial compression the buckling mode is always assumed to be $A_{11}\cos mx\cos ny$ (or $A_{11}\sin mx\sin ny$). Accordingly, for the post-buckling analysis of a DWCNT, we assume that the initial buckling mode is

$$w_I^{(2)}(x,y) = A_{11}^{(2)}\cos mx\cos ny + A_{02}^{(2)}\cos 2ny \tag{37a}$$

$$w_{II}^{(2)}(x,y) = a_{11}^{(2)}\cos mx\cos ny + a_{02}^{(2)}\cos 2ny \tag{37b}$$

in which $a_{11}^{(2)}/A_{11}^{(2)} = \chi_1$ is a constant, the details of which may be found in Ref. [33], from which one can see $\chi_1 < 1$, then inner tube has a lower amplitude than the outer tube.

It has been shown [33] that the effect of initial point defects in both outer and inner tubes is slightly large than that only in the outer tube. As a result, in the present study, the initial point defects are assumed to be in both outer and inner tubes, i.e., $W_I^* = W_{II}^* = W^*$. This initial local geometric imperfection is represented as a Fourier cosine series as

$$W^*(x,y,\varepsilon) = \varepsilon^2 a_m \exp(-\gamma_{C1}|x| - \gamma_{C2}|y|) = \varepsilon^2 \mu A_{11}^{(2)}\left(\frac{a_0}{2} + \sum_{i=1} a_i \cos ix\right)\left(\frac{b_0}{2} + \sum_{j=1} b_j \cos jy\right) \tag{38a}$$

where

$$a_i = \frac{4}{\pi}\int_0^{\pi/2} \exp(-\gamma_{C1}x)\cos ix dx,$$

$$b_j = \frac{2}{\pi}\int_0^{\pi} \exp(-\gamma_{C2}y)\cos jy dy \tag{38b}$$

and $\mu = a_m/A_{11}^{(2)}$ is the imperfection parameter.

Substituting Eqs. (34), (35), and (36*a*)–(36*c*) into Eqs. (23)–(30), and collecting terms of the same order of ε, we obtain three sets of perturbation equations for the regular and boundary layer solutions, respectively.

Then using Eqs. (37) and (38) to solve these perturbation equations of each order, and matching the regular solutions with the boundary layer solutions at each end of the shell, we obtain the asymptotic solutions W_I, F_I, Ψ_{xI}, and Ψ_{yI} for the outer tube, and W_{II}, F_{II}, Ψ_{xII}, and Ψ_{yII} for the inner tube, respectively (see Appendix A of Ref. [33] for details), from which one can see the prebuckling deformation of the tube is nonlinear.

Next, upon substitution of F_I and F_{II} into the boundary condition (31*d*) and F_I and W_I into closed condition (32) and Eq. (33*a*), the post-buckling equilibrium paths can be written as

$$\lambda_p = \lambda_p^{(0)} - \lambda_p^{(2)}(A_{11}^{(2)}\varepsilon)^2 + \lambda_p^{(4)}(A_{11}^{(2)}\varepsilon)^4 + \cdots \tag{39}$$

and

$$\delta_p = \delta_p^{(0)} - \delta_p^{(T)} + \delta_p^{(2)}(A_{11}^{(2)}\varepsilon)^2 + \delta_p^{(4)}(A_{11}^{(2)}\varepsilon)^4 + \cdots \tag{40}$$

It is noted that $\lambda_p^{(i)}$ and $\delta_p^{(i)}$ $(i=0,2,\ldots)$ are related to the material properties and are functions of temperature. In Eqs. (39) and (40), $(A_{11}^{(2)}\varepsilon)$ is taken as the second perturbation parameter relating to the dimensionless maximum deflection, and that can be expressed as

$$A_{11}^{(2)}\varepsilon = W_m - \Theta_1 W_m^2 + \cdots \tag{41}$$

where W_m is the dimensionless form of the maximum deflection of the outer tube that can be expressed as

$$W_m = \left[\frac{h}{[D_{11}^* D_{22}^* A_{11}^* A_{22}^*]^{1/4}}\frac{\bar{W}}{h} + \Theta_2\right] \tag{42}$$

All symbols used in Eqs. (39)–(42) are described in detail in the Appendix.

Equations (39)–(42) are employed to obtain numerical results for full nonlinear post-buckling load-shortening and load-deflection curves of DWCNTs embedded in an elastic matrix and subjected to axial compression in thermal environments, from which results for SWCNTs are obtained as a limiting case. Since the elastic foundation reacts in compression only, a possible uplifting region is expected. Because the contact region is not known at the outset, the solution procedure is complicated and therefore an iterative procedure is necessary to solve this nonlinear problem. In applying the contact condition, the shell panel area is discretized into a series of grids, and the contact status is assessed at each grid location. From Eq. (A11) in the Appendix one can see some equations, e.g., F_{00}, F_{02}, and F_{11}, involving K_1, K_2, and the contact function $H[W(x_g,y_g)]$, where $W(x_g,y_g)$ is the deflection at the grid coordinate (x_g,y_g) and summation is carried out over all grid coordinates by using the Gauss–Legendre quadrature procedure with Gauss weight assigned $C_g^{(M)}$. From convergence studies where the specific tolerance limit for F_{00}, F_{02}, and F_{11} is set to be less than 0.001, it is found that an acceptable accuracy for buckling load can be achieved by using 36×36 grid points, which is employed in Sec. 4.

The initial buckling load for a perfect double-walled carbon nanotube can readily be obtained numerically, by setting $\bar{W}^*/h = 0$ (or $\mu = 0$), while taking $\bar{W}/h = 0$ (note that $W_m \neq 0$). In this case, the minimum load (called buckling load) and corresponding buckling mode (m,n) can be determined by comparing loads (obtained from Eq. (39)) under various values of (m,n), which determine the number of half-waves in the X direction and of full waves in the Y direction.

4 Numerical Results and Discussion

Numerical results are presented in this section for perfect and imperfect, DWCNTs embedded in an elastic matrix subjected to axial compression. As argued before, the small scale effects must be considered in the buckling analysis. It should be noted that the material properties of CNTs are anisotropic, chirality-dependent, size-dependent, and temperature-dependent [35–40]. Also the buckling and post-buckling behavior of CNTs is very sensitive to the material properties and effective wall thickness [33,41]. Therefore, all effective material properties and wall thickness of a CNT need to be carefully determined, otherwise the results may be incorrect.

The molecular dynamics simulations are first carried out, the details of which may be found in Refs. [39,40]. From MD simulation results the temperature-dependent material properties for armchair (9,9) SWCNT and its two alternative DWCNTs [(4,4), (9,9)] and [(9,9), (14,14)] can be obtained numerically. The [(4,4), (9,9)]-tube is constructed by inserting (4,4) nanotube in the fiducial (9,9)-tube, while the [(9,9), (14,14)]-tube has the outer (14,14)-tube. Typical results are listed in Table 1 for (9,9)-, [(4,4), (9,9)]-, and [(9,9), (14,14)]-tubes with $L = 5.32$ nm under thermal environmental conditions $T = 300$, 700, and 1200 K. It is assumed that the distance between two adjacent walls remains unchanged and the intertube distance is taken to be 0.34 nm. It is noted that the effective wall thickness obtained for (9,9)-tube is $h = 0.066$ nm, while for [(4,4), (9,9)]- and [(9,9), (14,14)]-tubes is $h = 0.075$ nm.

The key issue for successful application of the nonlocal continuum mechanics models to CNTs is to determine the magnitude of the small scale parameter $e_0 a$. In the most studies e_0 is usually taken to be 0.39 proposed by Eringen [20]. However, there are no experiments conducted to determine the value of e_0 for CNTs. By

Table 1 Temperature-dependent material properties for CNTs (L=5.32 nm, ν_{12}=0.169)

Temperature (K)	E_{11} (TPa)	E_{22} (TPa)	G_{12} (TPa)	α_{11} ($\times 10^{-6}$/K)	α_{22} ($\times 10^{-6}$/K)
		(9,9)-tube (R=0.61 nm, h=0.066 nm)			
300	5.7911	7.9735	1.9840	2.9318	5.9864
700	5.5866	7.6920	1.9988	4.2143	4.6427
1200	5.4216	7.4647	2.0027	5.0511	3.9288
		[(4,4), (9,9)]-tube (R_{II}=0.27 nm, R_I=0.61 nm, h=0.075 nm)			
300	5.4824	7.5485	1.8610	2.9781	7.6158
700	5.3821	7.4103	1.8331	4.5280	6.6323
1200	5.2205	7.1878	1.7866	5.3393	5.7216
		[(9,9), (14,14)]-tube (R_{II}=0.61 nm, R_I=0.95 nm, h=0.075 nm)			
300	5.1054	7.0294	1.7912	3.0755	6.6412
700	4.9884	6.8683	1.7972	4.4475	6.5412
1200	4.7923	6.5983	1.7976	5.2503	6.4171

matching the theoretical buckling strain obtained by the nonlocal thin shell model to those from molecular mechanics simulations given by Sears and Batra [42], Zhang et al. [25] estimated $e_0 \cong 0.82$ and the small scale parameter e_0a is approximately 0.116 nm, by taking the characteristic length a as the length of carbon bond of 0.142 nm. Moreover, Zhang et al. [23] reported that e_0 varies from 0.546–1.043 for SWCNTs with different chiral angles. On the other hand, a conservative estimate of the small scale parameter e_0a is less than 2.0 nm for a SWCNT if the measured wave propagation frequency value for the SWCNT is greater than 10 THz [43]. In the present study, we give the estimation of parameter e_0a by matching the buckling loads of CNTs observed from the MD simulation results with the numerical results obtained from the nonlocal shear deformable shell model.

The buckling loads P_{cr} (in nano-Newtons) and corresponding critical strains for (9,9)-, [(4,4), (9,9)]-, and [(9,9), (14,14)]-tubes with L=5.32 nm under thermal environmental condition T=300, 700, and 1200 K are calculated and compared with MD simulation results in Table 2. Through comparison, we find that the buckling loads and corresponding critical strains obtained from the nonlocal shear deformable shell model and MD simulations can match very well if the small scale parameters are properly chosen, e.g., e_0a=0.0495 nm for the (9,9)-tube at T=300 K. It is clear that a large range of values for the small scale parameters e_0a is possible due to different CNTs, and these values will be used in all the following examples, except for Figs. 3(*a*) and 3(*b*).

Table 3 presents the buckling loads P_{cr} (in nano-Newtons) for (9,9)-, [(4,4), (9,9)]-, and [(9,9), (14,14)]-tubes embedded in an elastic matrix under axial compression in thermal environments T=300, 700, and 1200 K. The geometric parameters for the [(4,4), (9,9)]-tube are R_I=0.61 nm, R_{II}=0.27 nm, for the [(9,9), (14,14)]-tube are R_I=0.95 nm, R_{II}=0.61 nm, and each tube has the same thickness h=0.075 nm. By taking ε_0=2.39 meV and σ_0=0.341 nm, from Eq. (11), we have the van der Waals interaction constant C=58.6125 GPa/nm for the [(4,4), (9,9)]-tube and C=71.121 GPa/nm for the [(9,9), (14,14)]-tube. Three sets of foundation stiffness are considered. The stiffnesses are characterized by $(k_1,k_2)=(0.2,0)$ and (0.2, 0.02) for the weak foundation (like polymer matrix), by $(k_1,k_2)=(10,0)$ and (10, 1) for the medium foundation (like metal matrix), and by $(k_1,k_2)=(100,0)$ and (100, 10) for the hard foundation (like metal or ceramic matrix). Note that $(k_1,k_2)=(0,0)$ is for an unconstrained tube. The conventional Pasternak foundation, as previously used in Ref. [13], is included for direct comparison. It can be seen that the buckling loads for a tube resting on a tensionless Pasternak foundation are lower than those for a tube resting on a conventional Pasternak foundation. The percentage of the reduction is about 0.2%, 6%, and 27% for the [(9,9), (14,14)]-tube resting on a weak, medium and hard tensionless Pasternak foundation at the same thermal environmental condition. This means both conventional and tensionless Pasternak foundation models can well predict the buckling loads of CNTs embedded in polymer matrix. In contrast, the differences become pronounced when CNTs embedded in ceramic matrix. As in the case of unconstrained CNTs [33], the buckling loads are reduced with increases in temperature. The percentage of the reduction is about 6% and 12% for the [(9,9), (14,14)]-tube under T=700 and 1200 K, respectively. On the other hand, the buckling load of a CNT increases when it is embedded in an elastic matrix. The percentage of the increment is about 0.2%, 9%, and 71% for the [(9,9), (14,14)]-tube resting on a weak, medium and hard tensionless Pasternak foundation at T=300 K. It can

Table 2 Comparisons of buckling behavior for [(4,4),(9,9)], (9,9) and [(9,9), (14,14)] CNTs subjected to axial compression in thermal environments (L=5.32 nm, ν_{12}=0.169)

	[(4,4),(9,9)]-tube		(9,9)-tube		[(9,9), (14,14)]-tube	
	Critical strain	Buckling load P_{cr} (nN)	Critical strain	Buckling load P_{cr} (nN)	Critical strain	Buckling load P_{cr} (nN)
			T=300 K			
MD	0.0693	106.794	0.0528	79.430	0.0499	113.994
Shell model	0.0683	106.747(0.0343)[a]	0.0543	79.427(0.0495)	0.0502	113.999(0.0198)
			T=700 K			
MD	0.0682	106.272	0.0482	71.925	0.0475	107.615
Shell model	0.0677	106.263(0.0315)	0.0493	71.943(0.0643)	0.0470	107.618(0.0375)
			T=1200 K			
MD	0.0659	100.907	0.0452	66.749	0.0424	100.121
Shell model	0.0635	100.885(0.0356)	0.0443	66.763(0.0719)	0.0427	100.110(0.0487)

[a]The number in brackets indicate the value of e_0a (nm).

Table 3 Buckling loads P_{cr} (nN) for perfect CNTs embedded in an elastic matrix under axial compression in thermal environments

		[(4,4), (9,9)]-tube		(9,9)-tube		[(9,9), (14,14)]-tube	
Temperature	(k_1,k_2)	Conventional	Tensionless	Conventional	Tensionless	Conventional	Tensionless
$T=300$ K	(0, 0)	106.747	106.747	79.427	79.427	113.999	113.999
	(0.2, 0)	106.910	106.824	79.981	79.696	114.076	114.040
	(0.2, 0.02)	107.431	107.108	80.928	80.128	114.387	114.212
	(10, 0)	114.049	110.408	95.745	83.974	117.613	116.042
	(10, 1)	139.376	124.843	106.248	91.313	132.537	124.438
	(100, 0)	151.091	134.113	114.552	98.194	139.276	128.730
	(100, 10)	394.101	257.605	362.035	227.204	266.298	194.957
$T=700$ K	(0, 0)	106.263	106.263	71.943	71.943	107.618	107.618
	(0.2, 0)	106.429	106.341	72.492	72.206	107.683	107.652
	(0.2, 0.02)	106.954	106.633	73.422	72.608	107.982	107.817
	(10, 0)	113.926	110.228	85.205	73.920	110.822	109.331
	(10, 1)	139.466	124.293	99.978	83.419	124.361	116.564
	(100, 0)	153.277	134.500	103.586	88.361	128.887	119.621
	(100, 10)	398.198	257.163	342.505	212.002	255.099	185.351
$T=1200$ K	(0, 0)	100.885	100.885	66.763	66.763	100.110	100.110
	(0.2, 0)	101.054	100.965	67.308	67.019	100.159	100.131
	(0.2, 0.02)	101.582	101.256	68.222	67.397	100.420	100.259
	(10, 0)	108.218	104.661	70.295	68.533	102.316	101.093
	(10, 1)	133.674	119.212	94.190	77.680	115.256	107.627
	(100, 0)	144.095	127.492	96.624	81.755	117.865	109.665
	(100, 10)	390.352	249.702	335.152	204.338	243.211	175.828

also be seen that the buckling load of [(9,9), (14,14)]-tube with or without surrounding elastic medium is higher than that of (9,9)-tube, except for the case of $(k_1,k_2)=(100,10)$.

Figures 2(*a*) and 2(*b*) present the post-buckling load-shortening curves for a (9,9)-tube subjected to axial compression under thermal environmental conditions, and the results are compared with the MD simulation results under $T=300$ and 700 K. The temperature-dependent material properties are used in the present example as given in Table 1. They show that the present results based on a nonlocal shear deformable shell model are in good agreement with the MD simulation results when $e_0a=0.0495$ and 0.0643 nm, respectively. It is worthy to note that in the present example the tube radius-to-thickness ratio ($R/h=9.24$) is much smaller than 20, and in such a case the transverse shear deformation should be taken into account. In contrast, the classical shell theory will give higher buckling loads, as previously shown in Ref. [41].

Figures 3(*a*) and 3(*b*) show the effect of the small scale parameter e_0a (=0.0, 0.0495 and 0.116 nm) on the post-buckling behavior of (9,9)-tube subjected to axial compression under $T=300$ K. Here $e_0a=0$ means the local shear deformable shell model [33], and $e_0a=0.116$ nm denotes $e_0=0.82$ [25] when a is taken to be 0.142 nm. It can be seen that the tube will have much lower post-buckling equilibrium paths when $e_0a=0.116$ nm. In other words, the effect of the small scale on the post-buckling response becomes more significant as parameter e_0a becomes larger.

Figures 4(*a*) and 4(*b*) compare post-buckling responses of (9,9)-, [(4,4), (9,9)]-, and [(9,9), (14,14)]-tubes resting on a weak tensionless elastic foundation with $(k_1,k_2)=(0.2,0.02)$. It can be seen that the [(9,9), (14,14)]-tube has a high buckling load, whereas the [(4,4), (9,9)]-tube has a high buckling strain among the three. It can be seen that the post-buckling equilibrium path of (9,9)-tube is unstable, and in such a case imperfection sensitivity can be predicted. It can also be seen that an increase in load is usually required to obtain an increase in displacement for both [(9,9), (14,14)]-, and [(4,4), (9,9)]-tubes, and the [(4,4), (9,9)]-tube is much stiffer in the post-buckling region. This phenomenon is very similar to that observed in the buckling experiment re-

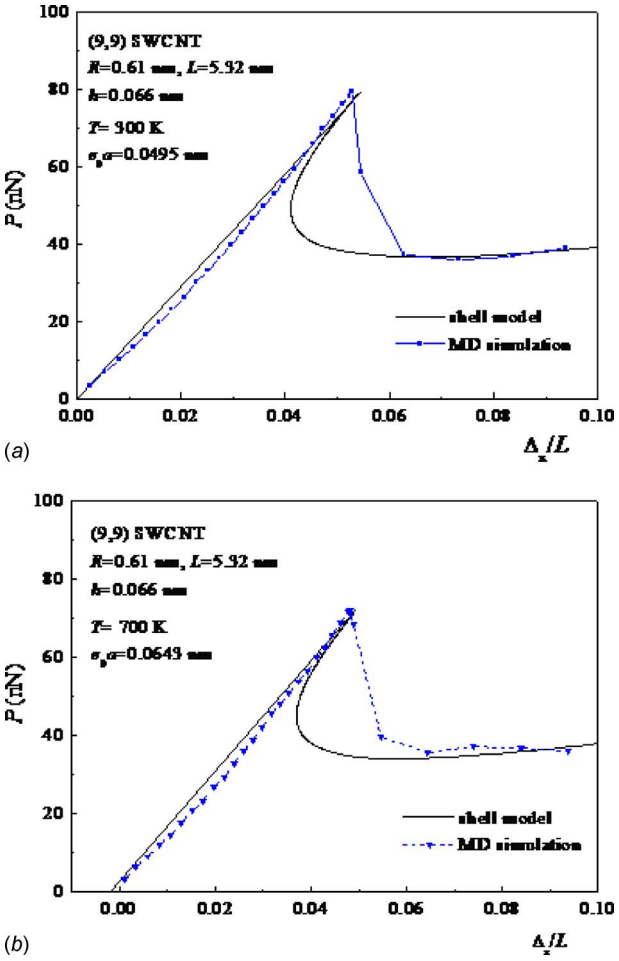

Fig. 2 Comparisons of post-buckling behavior for a (9,9)-tube under axial compression in thermal environments: (*a*) $T=300$ K and (*b*) $T=700$ K

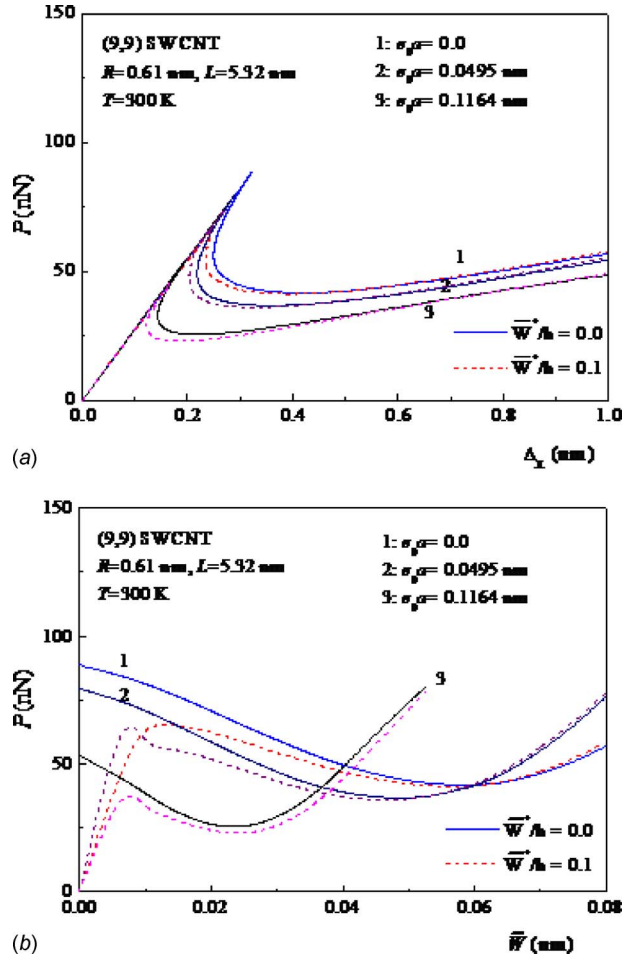

Fig. 3 Comparisons of post-buckling behavior of (9,9)-tube with different values of small scale parameter e_0a subjected to axial compression: (*a*) load-shortening and (*b*) load-deflection

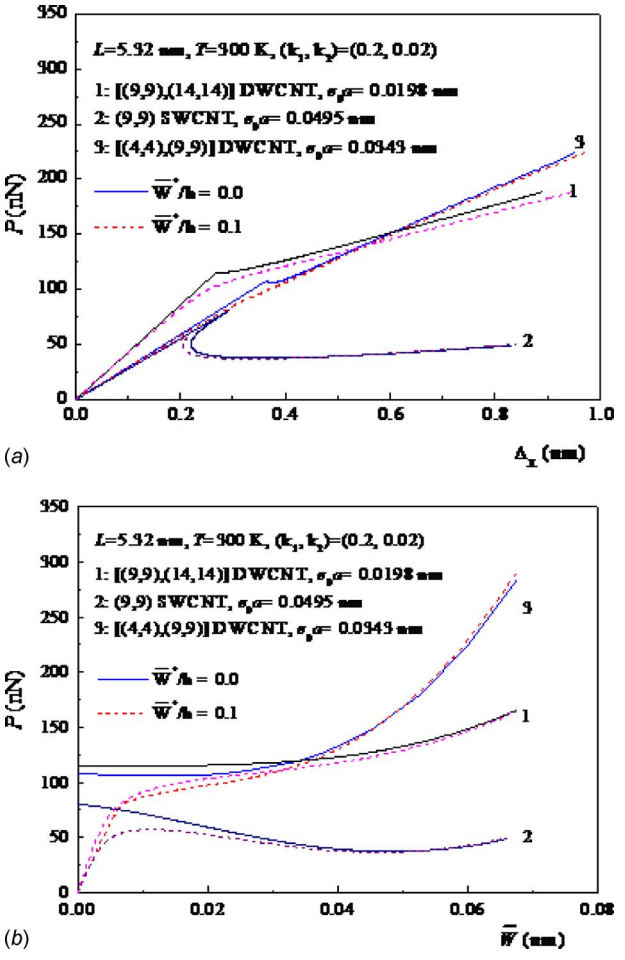

Fig. 4 Comparisons of post-buckling behavior for SWCNT and DWCNTs resting on tensionless elastic foundations: (*a*) load-shortening and (*b*) load-deflection

ported in Refs. [44,45]. In such a case, the post-buckling path is stable and the DWCNT is virtually imperfection-insensitive.

Figures 5(*a*) and 5(*b*) show the effect of the foundation stiffness on the post-buckling behavior of [(9,9), (14,14)]-tube subjected to axial compression under thermal environmental condition $T=300$ K resting on tensionless Pasternak foundations. Three different values of foundation stiffnesses $(k_1,k_2)=(0.2,0.02)$, (10, 1), and (100, 10) are considered. It can be seen that the tube resting on a hard elastic foundation has the highest buckling load and post-buckling strength. The increase in buckling load and post-buckling strength becomes greater as the foundation stiffness is increased, or vice versa.

Figures 6(*a*) and 6(*b*) compare the post-buckling behavior of [(9,9), (14,14)]-tube subjected to axial compression under thermal environmental condition $T=300$ K resting on conventional and tensionless elastic foundations. The results for the same unconstrained tube (referred to as "foundationless" in the figure) are also given as a comparator. The results show that the post-buckling load-deflection curve for the tube resting on a tensionless elastic foundation lies between the deflection curves of the unconstrained tube and the tube resting on a conventional elastic foundation. It can also be seen that the post-buckling strength of the tube resting on a hard tensionless elastic foundation is much lower than that of the tube resting on a conventional elastic foundation.

Figures 7(*a*) and 7(*b*) show the post-buckling responses of [(9,9), (14,14)]-tube under three different sets of thermal environmental conditions $T=300$, 700, and 1200 K, when the tube is unilaterally constrained by a hard tensionless elastic foundation with $(k_1,k_2)=(100,10)$. For these three thermal environmental cases $\chi_1=0.1562$, 0.1691, and 0.1840, respectively, and $\bar{W}_I-\bar{W}_{II}$ is definitely less than 0.425 nm in the post-buckling region, so that the linear function assumption for the van der Waals interaction force is reasonable. It is found that an initial extension occurs as the temperature increases and the buckling loads as well as post-buckling strength are reduced with increases in temperature. To compare with Figs. 6a and 6b of Ref. [33], it is found that the effect of temperature changes on the post-buckling behavior is more pronounced for CNTs resting on elastic foundations.

It is worthy to not that, in Figs. 3(*a*) and 3(*b*), the post-buckling deflection of the outer tube is less than 0.08 nm, and therefore, in most cases the tensile stresses due to van der Waals interaction do not occur between the matrix and CNT. The post-buckling load-shortening and load-deflection curves for imperfect CNTs have also been plotted in Figs. 3(*a*) and 3(*b*), in which $\bar{W}^*/h$ means the dimensionless form of the maximum initial geometric imperfection of the tube. The local imperfection parameters are taken to be $C_1/L=0.03$ and $C_2/R_I=0.3$.

5 Concluding Remarks

Post-buckling behavior of axially compressed DWCNTs embedded in an elastic matrix has been presented on the basis of the nonlocal shear deformable shell model. The surrounding elastic medium is modeled as a tensionless Pasternak foundation. The nonlinear prebuckling deformations of the shell and initial point defects are both taken into account. We considered the small scale

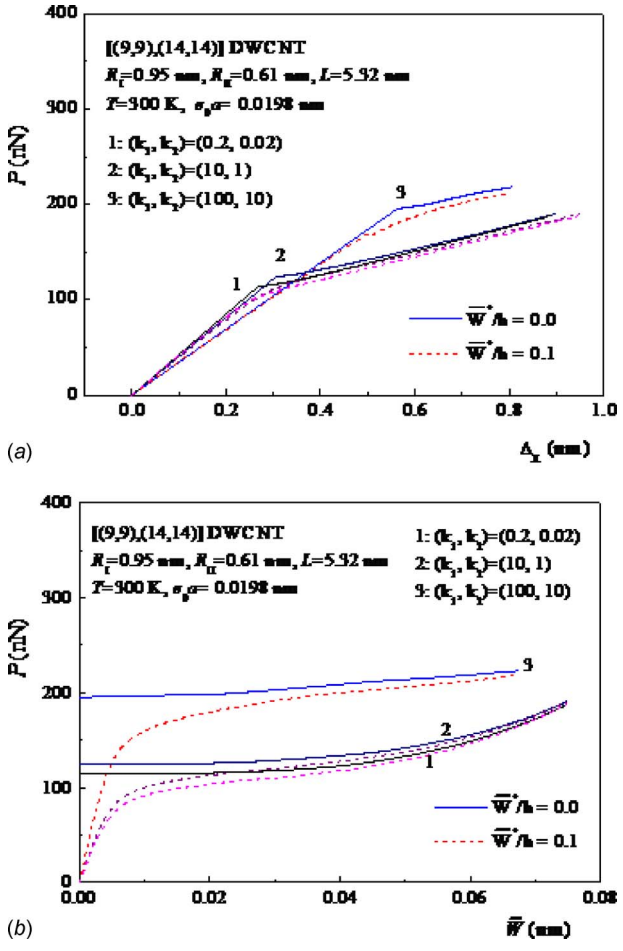

Fig. 5 Effect of the foundation stiffness on the post-buckling behavior of a [(9,9), (14,14)]-tube resting on tensionless elastic foundations: (*a*) load-shortening and (*b*) load-deflection

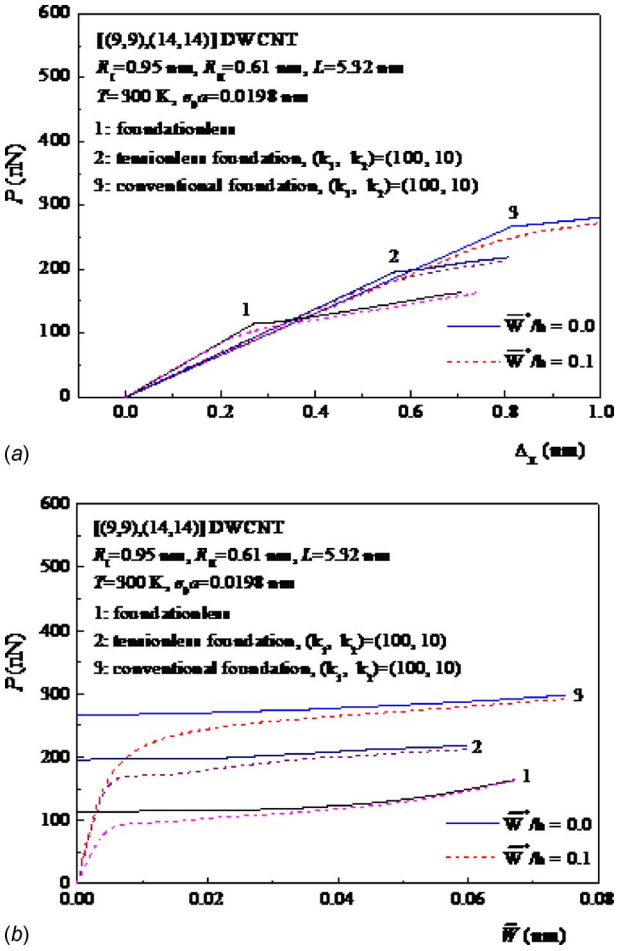

Fig. 6 Comparisons of post-buckling behavior for a [(9,9), (14,14)]-tube resting on different kinds of elastic foundations: (*a*) load-shortening and (*b*) load-deflection

effects in three ways, that is, the small scale parameter e_0a in governing Eqs. (2) and (6), size-dependent van der Waals interaction coefficient C calculated by Eq. (11), and size-dependent and temperature-dependent material properties obtained by MD simulations. The results show that buckling and post-buckling behavior of CNTs is very sensitive to the small scale parameter e_0a. The results reveal that the unilateral constraint has a significant effect on the post-buckling response of CNTs subjected to axial compression in thermal environments when the foundation stiffness is sufficiently large. They confirm that the temperature change only has a small effect on the post-buckling behavior of DWCNTs. They also confirm that both unilaterally constrained and unconstrained DWCNT have a stable post-buckling equilibrium path, and the structure is virtually imperfection-insensitive.

Acknowledgment

This work is supported in part by the National Natural Science Foundation of China under Grant No. 10802050. The authors are grateful for this financial support.

Appendix

In Eqs. (39)–(42) (with other symbols are defined as in Ref. [33])

$$\Theta_1 = \left[\gamma_{14}\gamma_{24} m^4 n^2 \beta^2 R_{02} \frac{g_{21}}{g_{06}} \varepsilon^{-1} + \frac{1}{8} n^2 \beta^2 \mu_{12} \varepsilon + 2 \frac{\gamma_5}{\gamma_{24}} J_{10} \lambda_B^{(2)} \right] \tag{A1}$$

$$\Theta_2 = \frac{J_{10}}{\gamma_{24}} [2\gamma_5 \lambda_B^{(0)} + (\gamma_{T2} - \gamma_5 \gamma_{T1}) \Delta T] \tag{A2}$$

$$\lambda_p^{(i)} = \frac{1}{1+\gamma_0} [\lambda_B^{(i)} + \gamma_0 \lambda_b^{(i)}] \quad (i = 0,2,4) \tag{A3}$$

where

$$\lambda_B^{(0)} = \frac{1}{2} \left\{ \frac{\gamma_{24} m^2}{g_{06} R_{11} \mu_{11}} \varepsilon^{-1} + \frac{1}{\gamma_{24} m^2 R_{11} \mu_{11}} [g_{08} + F_{11} R_{11} + C_0 R_{11} (1 - \chi_1)] \varepsilon \right\}$$

$$\lambda_B^{(2)} = \frac{1}{2} \left\{ \frac{2\gamma_{14}\gamma_{24}^2 m^6 n^4 \beta^4}{g_{06}^2 \mu_{11}} \frac{R_{11}+1}{R_{11}} R_{02} g_{21} \varepsilon^{-1} - \frac{1}{16\gamma_{24}} m^2 \mu_{12} \varepsilon + \frac{\gamma_{24} m^2 n^4 \beta^4}{4 g_{06}} \frac{g_{06}\mu_{122} + 8 m^4 R_{20} \mu_{124}}{g_{06} R_{11} \mu_{11} - 4 m^4 R_{20} \mu_{20}} \varepsilon - \frac{2\gamma_{24} m^2 n^4 \beta^4}{g_{06} \mu_{11}} C_0 \chi_1 (g_{21} - \gamma_0 g_{22} \mu_{11}) \varepsilon \right\}$$

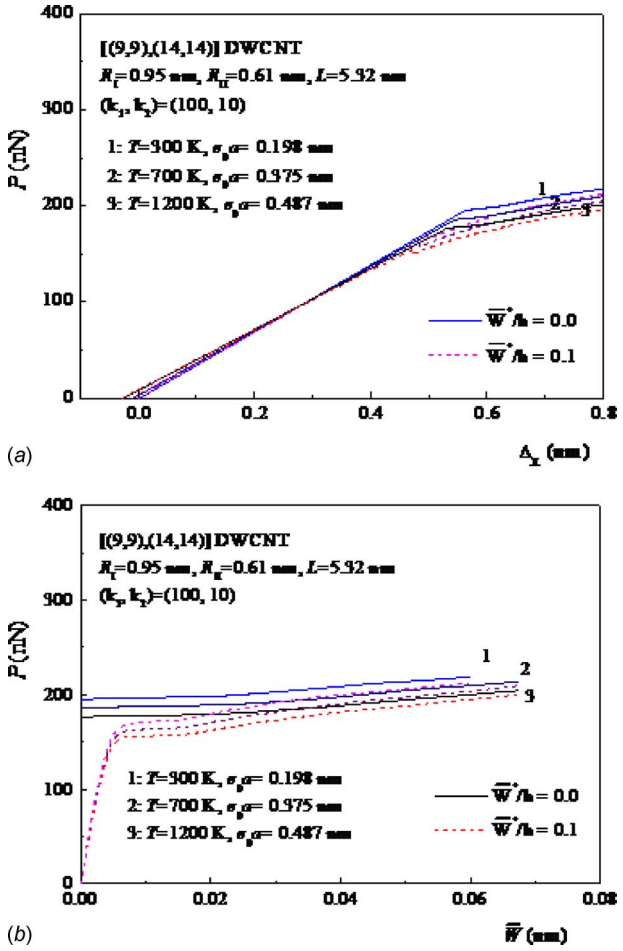

Fig. 7 The effect of temperature rise on the post-buckling behavior of a [(9,9), (14,14)]-tube resting on tensionless elastic foundations: (*a*) load-shortening and (*b*) load-deflection

$$\lambda_B^{(4)} = \frac{1}{2}\frac{4\gamma_{14}^2\gamma_{24}^3 m^{10}n^8\beta^8}{g_{06}^3}\left\{\frac{1}{\mu_{11}}\frac{2g_{136}R_{13}\mu_{13}+g_{06}\mu_{131}}{g_{136}R_{13}\mu_{13}-g_{06}R_{11}\mu_{11}}(R_{02}g_{21})^2 + \frac{g_{136}R_{13}\mu_{13}(R_{11}-1)+g_{06}\mu_{11}\mu_{133}}{g_{136}R_{13}\mu_{13}-g_{06}R_{11}\mu_{11}}[g_{21}g_{23}+\gamma_0\chi_1^2 g_{22}g_{20}] \times (R_{02})^2\mu_{144}\right\}\varepsilon^{-1} \quad \text{(A4)}$$

$$\lambda_b^{(0)} = \frac{1}{2}\left\{\frac{\gamma_{24}m^2}{\gamma_0^2 g_{06}R_{11}\mu_{11}}\varepsilon^{-1} + \frac{1}{\gamma_{24}m^2R_{11}\mu_{11}}\left[g_{08}-C_0R_{11}\frac{(1-\chi_1)}{\gamma_0\chi_1}\right]\varepsilon\right\}$$

$$\lambda_b^{(2)} = \frac{1}{2}\left\{\frac{2\gamma_{14}\gamma_{24}^2m^6n^4\beta^4}{\gamma_0 g_{06}^2\mu_{11}}\frac{R_{11}+1}{R_{11}}R_{02}g_{22}\varepsilon^{-1} - \frac{1}{16\gamma_{24}}\chi_1^2m^2\mu_{12}\varepsilon + \frac{\gamma_{24}m^2n^4\beta^4}{4g_{06}}\frac{g_{06}\mu_{122}+8m^4R_{20}\mu_{124}}{g_{06}R_{11}\mu_{11}-4m^4R_{20}\mu_{20}}\chi_1^2\varepsilon + \frac{2\gamma_{24}m^2n^4\beta^4}{\gamma_0\chi_1 g_{06}\mu_{11}}C_0(g_{21}\mu_{11}-\gamma_0 g_{22})\varepsilon\right\}$$

$$\lambda_b^{(4)} = \frac{1}{2}\frac{4\gamma_{14}^2\gamma_{24}^3 m^{10}n^8\beta^8}{g_{06}^3}\left\{\frac{1}{\mu_{11}}\frac{2g_{136}R_{13}\mu_{13}+g_{06}\mu_{131}}{g_{136}R_{13}\mu_{13}-g_{06}R_{11}\mu_{11}}(R_{02}g_{22})^2 + \frac{g_{136}R_{13}\mu_{13}(R_{11}-1)+g_{06}\mu_{11}\mu_{133}}{g_{136}R_{13}\mu_{13}-g_{06}R_{11}\mu_{11}}[g_{20}g_{21}+\gamma_0\chi_1^2 g_{22}g_{24}] \times (R_{02})^2\mu_{144}\right\}\varepsilon^{-1} \quad \text{(A5)}$$

$$\delta_p^{(0)} = \frac{1}{\gamma_{24}}\left(\gamma_{24}^2 - \frac{\gamma_5^2}{\pi\vartheta}\varepsilon^{1/2} - \frac{\gamma_5^2}{\gamma_{14}\gamma_{24}}[C_0(1-\chi_1)+F_{00}]\varepsilon^2\right)\lambda_B \quad \text{(A6)}$$

$$\delta_p^{(T)} = \frac{1}{2\gamma_{24}}\left\{(\gamma_{24}^2\gamma_{T1}-\gamma_5\gamma_{T2}) + \frac{\gamma_5}{\pi\vartheta}(\gamma_{T2}-\gamma_5\gamma_{T1})\varepsilon^{1/2} + \frac{\gamma_5}{\gamma_{14}\gamma_{24}}(\gamma_{T2}-\gamma_5\gamma_{T1})[C_0(1-\chi_1)+F_{00}]\varepsilon^2\right\}\Delta T \quad \text{(A7)}$$

$$\delta_p^{(2)} = \tfrac{1}{16}m^2\mu_{12}\varepsilon \quad \text{(A8)}$$

$$\delta_p^{(4)} = \left\{\frac{1}{16}\frac{\vartheta}{\pi}\frac{\gamma_{14}^2\gamma_{24}^2m^8n^4\beta^4}{g_{06}^2}(R_{02}g_{21})^2\varepsilon^{-3/2} + \frac{m^2n^4\beta^4}{128}\left[\frac{g_{06}\mu_{12}+8m^4R_{20}\mu_{11}}{g_{06}R_{11}\mu_{11}-4m^4R_{20}\mu_{20}}\right]^2R_{11}^2\mu_{11}^2\varepsilon^3\right\} \quad \text{(A9)}$$

and in Eq. (A6) λ_B is the dimensionless axial stress of outer tube and can be written as

$$\lambda_B = \lambda_B^{(0)} - \lambda_B^{(2)}(A_{11}^{(2)}\varepsilon)^2 + \lambda_B^{(4)}(A_{11}^{(2)}\varepsilon)^4 + \cdots \quad \text{(A10)}$$

where $(A_{11}^{(2)}\varepsilon)$ is defined by Eq. (41), and in the above equations

$$F_{00} = \sum_{g=0}^{M} C_g^{(M)}H[W(x_g,y_g)]K_1,$$

$$F_{02} = \sum_{g=0}^{M} C_g^{(M)}H[W(x_g,y_g)][K_1+K_2 4n^2\beta^2]$$

$$F_{11} = \sum_{g=0}^{M} C_g^{(M)}H[W(x_g,y_g)][K_1+K_2(m^2+n^2\beta^2)]$$

$$J_{10} = 1 - \frac{1}{\gamma_{14}\gamma_{24}}[C_0(1-\chi_1)+F_{00}]\varepsilon^2,$$

$$J_{22} = (\gamma_{114}+\gamma_{133}g_{41})16n^4\beta^4 + C_0R_{02} + F_{02}R_{02}$$

$$g_{20} = \frac{C_0R_{02}}{[\gamma_0(\gamma_{114}+\gamma_{133}g_{41})16n^4\beta^4+C_0R_{02}]J_{22}-(C_0R_{02})^2}$$

$$g_{21} = \frac{[\gamma_0(\gamma_{114}+\gamma_{133}g_{41})16n^4\beta^4+C_0R_{02}]+\chi_1^2C_0R_{02}}{[\gamma_0(\gamma_{114}+\gamma_{133}g_{41})16n^4\beta^4+C_0R_{02}]J_{22}-(C_0R_{02})^2}\mu_{11}$$

$$g_{22} = \frac{\chi_1^2J_{22}+C_0R_{02}}{[\gamma_0(\gamma_{114}+\gamma_{133}g_{41})16n^4\beta^4+C_0R_{02}]J_{22}-(C_0R_{02})^2}\mu_{11}$$

$$g_{23} = \frac{[\gamma_0(\gamma_{114}+\gamma_{133}g_{41})16n^4\beta^4+C_0R_{02}]}{[\gamma_0(\gamma_{114}+\gamma_{133}g_{41})16n^4\beta^4+C_0R_{02}]J_{22}-(C_0R_{02})^2}$$

$$g_{24} = \frac{J_{22}}{[\gamma_0(\gamma_{114}+\gamma_{133}g_{41})16n^4\beta^4+C_0R_{02}]J_{22}-(C_0R_{02})^2}$$

$$R_{11} = 1+\tau^2\pi^2(m^2+n^2\beta^2), \quad R_{13} = 1+\tau^2\pi^2(m^2+9n^2\beta^2)$$

$$R_{20} = 1+\tau^2\pi^2 4m^2, \quad R_{02} = 1+\tau^2\pi^2 4n^2\beta^2$$

$$\mu_{122} = 2R_{11}\mu_{11}^2 + \mu_{12}\mu_{120}/\mu_{11} + (R_{11}+R_{20})\mu_{12}\mu_{20},$$

$$\mu_{124} = R_{11}\mu_{11}\mu_{20} + \mu_{120}$$

$$\mu_{144} = \mu_{02} + \mu_{102}/(R_{11}\mu_{11}),$$

$$\mu_{131} = \mu_{11}\mu_{13}(R_{13}+1) + \mu_{11}R_{11}(R_{13}-1)$$

$$\mu_{133} = R_{11}(R_{13} + 1) + \mu_{13}(R_{11} + R_{13}) \tag{A11}$$

References

[1] Liu, B., Jiang, H., Johnson, H. T., and Huang, Y., 2004, "The Influence of Mechanical Deformation on the Electrical Properties of Single Wall Carbon Nanotubes," J. Mech. Phys. Solids, **52**, pp. 1–26.

[2] Jiang, H., Liu, B., Huang, Y., and Hwang, K. C., 2004, "Thermal Expansion of Single Wall Carbon Nanotubes," ASME J. Eng. Mater. Technol., **126**, pp. 265–270.

[3] Yakobson, B. I., Brabec, C. J., and Bernholc, J., 1996, "Nanomechanics of Carbon Tubes: Instability Beyond Linear Response," Phys. Rev. Lett., **76**, pp. 2511–2514.

[4] Lourie, O., Cox, D. M., and Wagner, H. D., 1998, "Buckling and Collapse of Embedded Carbon Nanotubes," Phys. Rev. Lett., **81**, pp. 1638–1641.

[5] Zhang, W., Suhr, J., and Koratkar, N. A., 2006, "Observation of High Buckling Stability in Carbon Nanotube Polymer Composites," Adv. Mater., **18**, pp. 452–456.

[6] Hadjiev, V. G., Lagoudas, D. C., Oh, E.-S., Thakre, P., Davis, D., Files, B. S., Yowell, L., Arepalli, S., Bahr, J. L., and Tour, J. M., 2006, "Buckling Instabilities of Octadecylamine Functionalized Carbon Nanotubes Embedded in Epoxy," Compos. Sci. Technol., **66**, pp. 128–136.

[7] Ru, C. Q., 2001, "Axially Compressed Buckling of a Doublewalled Carbon Nanotube Embedded in an Elastic Medium," J. Mech. Phys. Solids, **49**, pp. 1265–1279.

[8] Ranjbartoreh, A. R., Ghorbanpour, A., and Soltani, B., 2007, "Double-Walled Carbon Nanotube With Surrounding Elastic Medium Under Axial Pressure," Physica E (Amsterdam), **39**, pp. 230–239.

[9] Yang, H. K., and Wang, X., 2007, "Torsional Buckling of Multi-Wall Carbon Nanotubes Embedded in an Elastic Medium," Compos. Struct., **77**, pp. 182–192.

[10] Yang, H. K., and Wang, X., 2006, "Bending Stability of Multi-Wall Carbon Nanotubes Embedded in an Elastic Medium," Modell. Simul. Mater. Sci. Eng., **14**, pp. 99–116.

[11] Zhang, Y. Q., Liu, G. R., Qiang, H. F., and Li, G. Y., 2006, "Investigation of Buckling of Double-Walled Carbon Nanotubes Embedded in an Elastic Medium Using the Energy Method," Int. J. Mech. Sci., **48**, pp. 53–61.

[12] Wang, X., Lu, G., and Lu, Y. J., 2007, "Buckling of Embedded Multi-Walled Carbon Nanotubes Under Combined Torsion and Axial Loading," Int. J. Solids Struct., **44**, pp. 336–351.

[13] Kitipornchai, S., He, X. Q., and Liew, K. M., 2005, "Buckling Analysis of Triple-Walled Carbon Nanotubes Embedded in an Elastic Matrix," J. Appl. Phys., **97**, p. 114318.

[14] Jiang, L. Y., Huang, Y., Jiang, H., Ravichandran, G., Gao, H., Hwang, K. C., and Liu, B., 2006, "A Cohesive Law for Carbon Nanotube/Polymer Interfaces Based on the van der Waals Force," J. Mech. Phys. Solids, **54**, pp. 2436–2452.

[15] Girifalco, L. A., and Lad, R. A., 1956, "Energy of Cohesion, Compressibility, and the Potential Energy Functions of Graphite System," J. Chem. Phys., **25**, pp. 693–697.

[16] Girifalco, L. A., 1991, "Interaction Potential for C_{60} Molecules," J. Phys. Chem., **95**, pp. 5370–5371.

[17] He, X. Q., Kitipornchai, S., and Liew, K. M., 2005, "Buckling Analysis of Multi-Walled Carbon Nanotubes: A Continuum Model Accounting for van der Waals Interaction," J. Mech. Phys. Solids, **53**, pp. 303–326.

[18] Shen, H.-S., 2004, "Postbuckling Prediction of Double-Walled Carbon Nanotubes Under Hydrostatic Pressure," Int. J. Solids Struct., **41**, pp. 2643–2657.

[19] Wu, J., Hwanga, K. C., and Huang, Y., 2008, "An Atomistic-Based Finite-Deformation Shell Theory for Single-Wall Carbon Nanotubes," J. Mech. Phys. Solids, **56**, pp. 279–292.

[20] Eringen, A. C., 1983, "On Differential Equations of Nonlocal Elasticity and Solutions of Screw Dislocation and Surface Waves," J. Appl. Phys., **54**, pp. 4703–4710.

[21] Zhang, Y. Q., Liu, G. R., and Wang, J. S., 2004, "Small-Scale Effects on Buckling of Multiwalled Carbon Nanotubes Under Axial Compression," Phys. Rev. B, **70**, p. 205430.

[22] Zhang, Y. Q., Liu, G. R., and Han, X., 2006, "Effect of Small Length Scale on Elastic Buckling of Multi-Walled Carbon Nanotubes Under Radial Pressure," Phys. Lett. A, **349**, pp. 370–376.

[23] Zhang, Y. Y., Tan, V. B. C., and Wang, C. M., 2006, "Effect of Chirality on Buckling Behavior of Single-Walled Carbon Nanotube," J. Appl. Phys., **100**, p. 074304.

[24] Li, R., and Kardomateas, G. A., 2007, "Thermal Buckling of Multi-Walled Carbon Nanotubes by Nonlocal Elasticity," ASME J. Appl. Mech., **74**, pp. 399–405.

[25] Zhang, Y. Q., Liu, G. R., and Xie, X. Y., 2005, "Free Transverse Vibration of Double-Walled Carbon Nanotubes Using a Theory of Nonlocal Elasticity," Phys. Rev. B, **71**, p. 195404.

[26] Wang, Q., and Varadan, V. K., 2007, "Application of Nonlocal Elastic Shell Theory in Wave Propagation Analysis of Carbon Nanotubes," Smart Mater. Struct., **16**, pp. 178–190.

[27] Hu, Y.-G., Liew, K. M., Wang, Q., He, X. Q., and Yakobson, B. I., 2008, "Nonlocal Shell Model for Elastic Wave Propagation in Single- and Double-Walled Carbon Nanotubes," J. Mech. Phys. Solids, **56**, pp. 3475–3485.

[28] Zhang, P., Huang, Y., Geubelle, P. H., Klein, P. A., and Hwang, K. C., 2002, "The Elastic Modulus of Single-Wall Carbon Nanotubes: A Continuum Analysis Incorporating Interatomic Potentials," Int. J. Solids Struct., **39**, pp. 3893–3906.

[29] Jiang, H., Feng, X.-Q., Huang, Y., Hwang, K. C., and Wu, P. D., 2004, "Defect Nucleation in Carbon Nanotubes Under Tension And Torsion: Stone–Wales Transformation," Comput. Methods Appl. Mech. Eng., **193**, pp. 3419–3429.

[30] Reddy, J. N., and Liu, C. F., 1985, "A Higher-Order Shear Deformation Theory of Laminated Elastic Shells," Int. J. Eng. Sci., **23**, pp. 319–330.

[31] Shen, H.-S., 2001, "Postbuckling of Shear Deformable Cross-Ply Laminated Cylindrical Shells Under Combined External Pressure and Axial Compression," Int. J. Mech. Sci., **43**, pp. 2493–2523.

[32] Wang, C. Y., Ru, C. Q., and Mioduchowski, A., 2003, "Axially Compressed Buckling of Pressured Multiwall Carbon Nanotubes," Int. J. Solids Struct., **40**, pp. 3893–3911.

[33] Shen, H.-S., and Zhang, C.-L., 2006, "Postbuckling Prediction of Axially Loaded Double-Walled Carbon Nanotubes With Temperature Dependent Properties and Initial Defects," Phys. Rev. B, **74**, p. 035410.

[34] Zhou, O., 1994, "Defects in Carbon Nanostructures," Science, **263**, pp. 1744–1747.

[35] Jin, Y., and Yuan, F. G., 2003, "Simulation of Elastic Properties of Single-Walled Carbon Nanotubes," Compos. Sci. Technol., **63**, pp. 1507–1515.

[36] Elliott, J. A., Sandler, J. K. W., Windle, A. H., Young, R. J., and Shaffer, M. S. P., 2004, "Collapse of Single-Wall Carbon Nanotubes is Diameter Dependent," Phys. Rev. Lett., **92**, p. 095501.

[37] Wang, L., Zheng, Q., Liu, J. Z., and Jinag, Q., 2005, "Size Dependence of the Thin-Shell Model for Carbon Nanotubes," Phys. Rev. Lett., **95**, p. 105501.

[38] Chang, T., Geng, J., and Guo, X., 2005, "Chirality- and Size-Dependent Elastic Properties of Single-Walled Carbon Nanotubes," Appl. Phys. Lett., **87**, p. 251929.

[39] Zhang, C.-L., and Shen, H.-S., 2006, "Temperature-Dependent Elastic Properties of Single-Walled Carbon Nanotubes: Prediction From Molecular Dynamics Simulation," Appl. Phys. Lett., **89**, p. 081904.

[40] Zhang, C.-L., and Shen, H.-S., 2008, "Predicting the Elastic Properties of Double-Walled Carbon Nanotubes by Molecular Dynamics Simulation," J. Phys. D, **41**, p. 055404.

[41] Shen, H.-S., and Zhang, C.-L., 2007, "Postbuckling of Double-Walled Carbon Nanotubes With Temperature Dependent Properties and Initial Defects Under Combined Axial and Radial Mechanical Loads," Int. J. Solids Struct., **44**, pp. 1461–1487.

[42] Sears, A., and Batra, R. C., 2004, "Macroscopic Properties of Carbon Nanotubes From Molecular-Mechanics Simulations," Phys. Rev. B, **69**, p. 235406.

[43] Wang, Q., 2005, "Wave Propagation in Carbon Nanotubes via Nonlocal Continuum Mechanics," J. Appl. Phys., **98**, p. 124301.

[44] Waters, J. F., Riester, L., Jouzi, M., Guduru, P. R., and Xu, J. M., 2004, "Buckling Instabilities in Multiwalled Carbon Nanotubes Under Uniaxial Compression," Appl. Phys. Lett., **85**, pp. 1787–1789.

[45] Waters, J. F., Guduru, P. R., Jouzi, M., Xu, J. M., Hanlon, T., and Suresh, S., 2005, "Shell Buckling of individual Multiwalled Carbon Nanotubes Using Nanoindentation," Appl. Phys. Lett., **87**, p. 103109.